



Unsymmetrical hot electron heating in quasi-ballistic nanocontacts

Makusu Tsutsui, Tomoji Kawai & Masateru Taniguchi

The Institute of Scientific and Industrial Research, Osaka University, 8-1 Mihogaoka, Ibaraki, Osaka 567-0047, Japan.

SUBJECT AREAS:

ELECTRONIC MATERIALS
AND DEVICES

ATOMIC AND MOLECULAR
PHYSICS

QUANTUM PHYSICS

STATISTICAL PHYSICS,
THERMODYNAMICS AND
NONLINEAR DYNAMICS

Received

5 October 2011

Accepted

16 December 2011

Published

10 January 2012

Correspondence and
requests for materials
should be addressed to
M.T. (taniguti@sanken.
osaka-u.ac.jp)

Electrons are allowed to pass through a single atom connected to two electrodes without being scattered as the characteristic size is much smaller than the inelastic mean free path. In this quasi-ballistic regime, it is difficult to predict where and how power dissipation occurs in such current-carrying atomic system. Here, we report direct assessment of electrical heating in a metallic nanocontact. We find asymmetric electrical heating effects in the essentially symmetric single-atom contact. We simultaneously identified the voltage polarity independent onset of the local heating by conducting the inelastic noise spectroscopy. As a result, we revealed significant heat dissipation by hot electrons transmitting ballistically through the junction that creates a hot spot at the current downstream. This technique can be used as a platform for studying heat dissipation and transport in atomic/molecular systems.

Understanding and control of heat dissipation in nanoscale structures is one of the key issues in development of atomic- and molecular-scale electronics^{1–4}. Unlike diffusive electron transport in macroscopic systems, electronic charges are allowed to transmit through conductors without being scattered by phonons or defects when the characteristic size is much smaller than the inelastic mean free path. Energy dissipation in this quasi-ballistic regime is still non-negligible because of the huge current density that leads to relatively high electron-phonon scattering rates in the microstructures^{5–10}. This has been elucidated by recent experiments that report substantial local heating in current-carrying atomic and molecular junctions^{11–16}.

In contrast, little attention has been paid to power dissipation via hot electrons escaping through a quasi-ballistic contact under high field^{3,17}, which is of practical importance from viewpoint of assessing energy efficiency and current carrying capacity of atomic/molecular electronic devices. In the present work, therefore, we developed a micro-fabricated temperature sensing system for exploring electrical heating in Au single atom contacts. The operational principle is based on a mechanically-controllable break junction (MCBJ), a well-established method widely used for forming stable atom-sized junctions^{18,19}. Our idea here is to embed a lithographically-defined resistance thermometer²⁰ in MCBJs and utilize it to measure the local temperature at the banks of the free-standing single-atom contact under a current flow.

Results

The configuration of a temperature-sensor-integrated MCBJ is shown in Fig. 1 a–d (see also Methods). It consists of a free-standing Au nano-junction and adjacent Pt coils that serve as a resistance thermometer. The device architecture is designed to achieve a high sensitivity for local temperature measurements. The Pt sensing elements are thermally coupled to the junction via the underlying Al₂O₃ layer. Furthermore, Pt and Au leads were made partially free-standing for the sake of minimizing heat escape from the square Al₂O₃ regions. The whole structure was fabricated on a thick polyimide layer possessing excellent thermal insulating characteristics (thermal conductivity is about 0.3 W/mK, two orders of magnitude lower than that of Al₂O₃) to prevent heat leakage to the substrate.

The sensitivity of the micro-thermometers was evaluated by examining Joule heating at the Pt coil heater and characterizing the temperature change using the Pt thermometer on the other side of the Au nano-junction exploiting the temperature response of the resistance R_h and R_t of the heater and the thermometer, respectively (Fig. 2 a) and the calibration curve (Fig. 2 b) for converting $R_{h(t)}$ to $T_{h(t)}$ of the heater (thermometer) through the temperature coefficient r (see Methods for calibration of Pt resistance thermometer). Specifically, we measured R_h under a linear voltage sweep from $V_h = -0.8$ V to 0.8 V applied to the heater at a rate of 2 mV/s and simultaneously recorded R_t using the lock-in technique with the ac voltage V_{ac} of 2 mV at 1 kHz for a closed Au junction at $T_0 = 150$ K. The $R_h - V_h$ as well as $R_t - V_h$ characteristics reveal a parabolic feature (Fig. 2 c and e). We deduced a

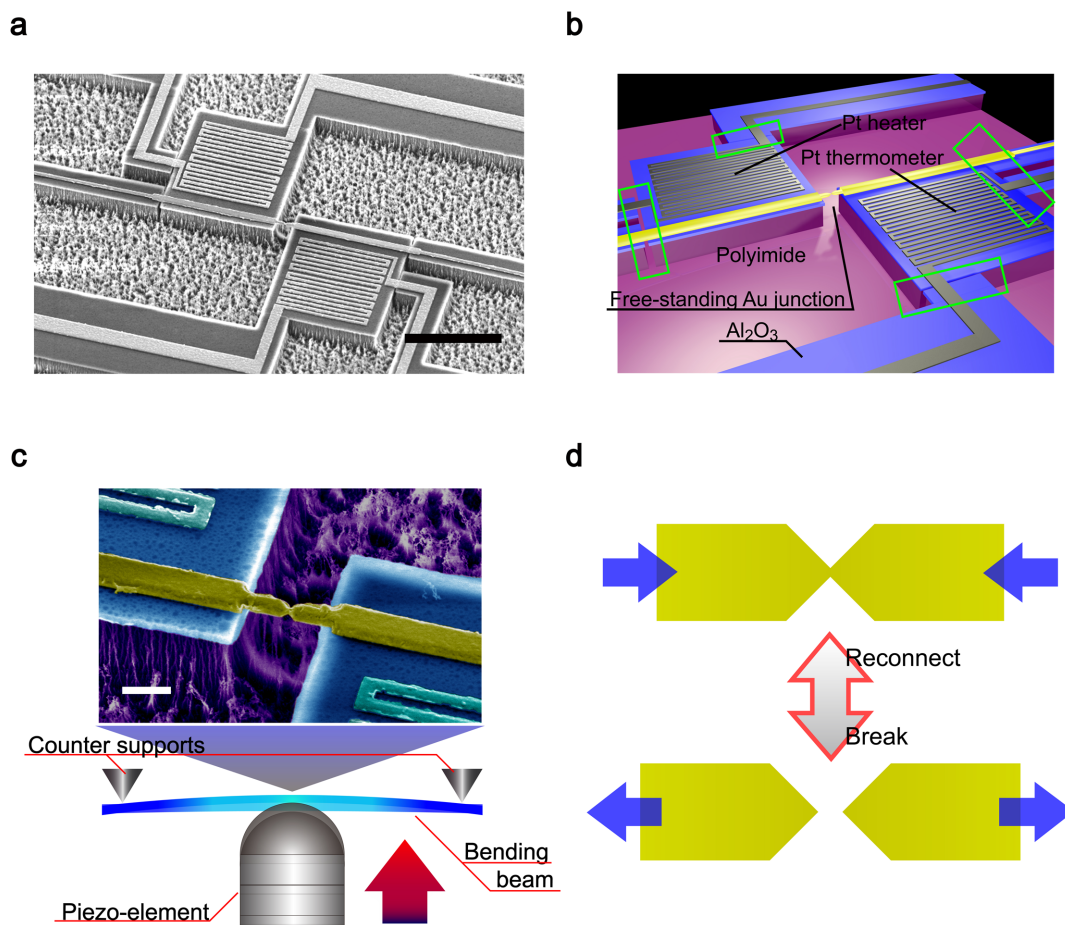


Figure 1 | Structure and operational principle of a micro-thermometer-embedded mechanically-controllable break junction (MCBJ). (a,b) A scanning electron microscopy image (a) and a schematic layout of a thermometer-integrated MCBJ (b). The device consists of a free-standing Au nano-junction and two adjacent Pt coils that function as a heater and a resistance thermometer. The alumina layers thermally connect the junction and the Pt coils. Regions marked by green rectangles possess free-standing structure. Scale bar is 10 μm . (c) A three-point bending configuration used for break junction experiments. Scale bar in the magnified view of a Au nanobridge is 1 μm . (d) The Au contact can be broken and re-formed by manipulating the beam bending.

temperature rise at the heater ΔT_h and the thermometer ΔT_t from the Joule heating-induced increase in the resistivity through $\Delta T_{h(t)} = (R_{h(t)} - R_0) / r$ (R_0 is the residual resistance estimated by extrapolating the $R_{h(t)} - T_0$ curve to $T_0 = 0$ K), which is valid in the present condition wherein $f \gg 2\pi\tau$ where $f = 1$ kHz is the voltage modulation frequency and τ is the thermal time constant, and plotted as a function of the dissipated power in the Pt heater $P_h = V_h^2 / R_h$ (Fig. 2 d and f). We see that ΔT_h and ΔT_t scale linearly with P_h . This suggests steady-state power dissipation and a certain level of heat diffusion from the heater to the thermometer via the Au junction²¹. The fact that ΔT_h is more than one order of magnitude higher than ΔT_t infers only a limited amount of heat transfer across the free-standing nano-junction due to the relatively small thermal conductance compared to that of the Au and Pt micro-leads.

The local temperature measurements were applied to detect Joule heat generated in a Au nano-junction at $T_0 = 150$ K. The wire resistance R_{Au} was obtained by the ac method utilizing the ac voltage V_{ac} of 2 mV at 1 kHz in a voltage range from $V_{Au} = -0.05$ V to 0.05 V (Fig. 3 a). We observed a non-linear increase in R_{Au} with $|V_{Au}|$ associated with electrical heating (Fig. 3 b). It is noticeable that $R_{Au} - V_{Au}$ characteristics is asymmetric with respect to the bias polarity. This behavior is ascribed to annealing effects on the micro-structure such as grain size and defect density and accompanied irreversible change in the electrical conductivity by Joule heating²². Heat

dissipation in the Au bridge led to concurrent rise in the resistance of the adjacent Pt thermometer as presented in Fig. 3 c. In accordance to the $R_{Au} - V_{Au}$ characteristics, R_t (and equivalently the local temperature at the thermometer) demonstrated irregular increase with V_{Au} , further suggesting structure deformation in the Au contact during electrical heating²². Meanwhile, $T_t - P_{Au}$ plots reveal linear feature that manifests diffusive transport in the Au nano-contacts and Joule heating origin of the local temperature increase at the thermometer, where $P_{Au} = V_{Au}^2 / R_{Au}$ is the power dissipated in Au nano-junctions (Fig. 3 d)²¹.

Having verified the adequate sensitivity of the micro-thermometer for detecting Joule heat occurring in the Au nano-bridge, we extended the power dissipation characterization to a single-atom chain (Fig. 4 a). After forming and holding a Au single atom contact at $T_0 = 80$ K (Fig. 4 b, see also Methods), we performed simultaneous measurements of $I - V_{Au}$ characteristics and the thermometer resistance. As the atomic contact tend to become unstable under elevated field by the local heating and current-induced forces, a small bias ramp of $V_{Au} \leq 0.1$ V was used (Fig. 4 a). Furthermore, we collected 10 points of I and R_t at each 0.2 mV step of V_{Au} for better resolution of the temperature sensor in the low-power regime. The resulting ramp rate was 0.2 mV/s. We calculated the average current $\langle I \rangle$ and the thermometer resistance $\langle R_t \rangle$ from the 10-point data. A linear $\langle I \rangle - V_{Au}$ curve was obtained reflecting ballistic electron

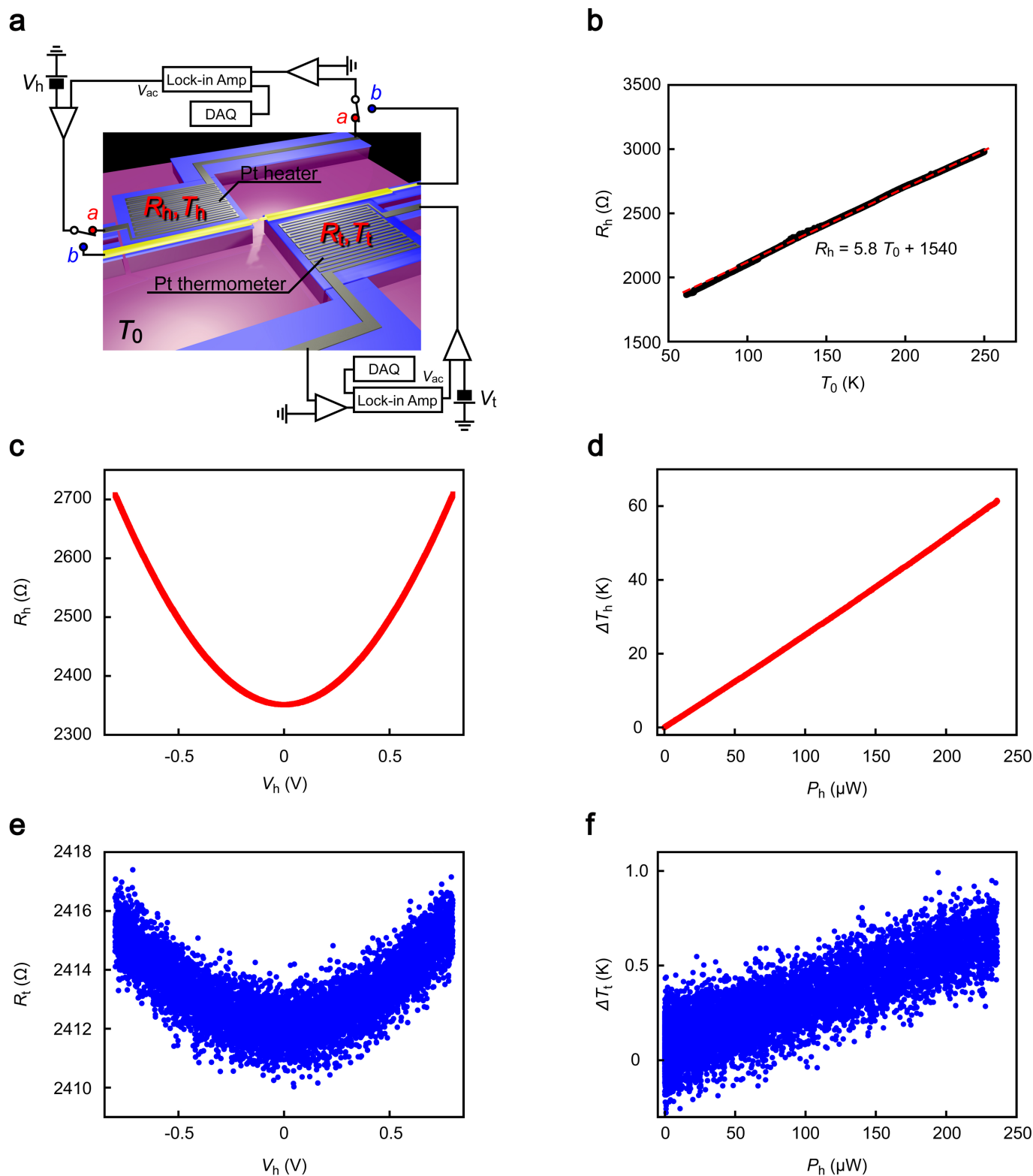


Figure 2 | Detection of Joule heat generated at a micro-heater. (a) A circuit used for the local temperature measurements. The lock-in amplifiers are employed to measure the resistance of the Pt coils. The circuit can also be utilized for measuring the resistance of the Au junction by turning the switch from *a* to *b*. (b) A calibration curve of the Pt thermometer. (c,d) Increase in the resistance of Pt heater R_h during a bias ramp plotted as a function of the applied dc voltage V_h (c) and corresponding temperature rise ΔT_h depicted as a function of power P_h consumed by the heater (d). (e,f) A concomitant change in the Pt thermometer resistance R_t (e) and corresponding temperature rise ΔT_t depicted as a function of power P_h that indicates an increase of the local temperature at the thermometer by heat transfer from the heater via the Au nanobridge (f).

transport through the Au single-atom chain (Fig. 4 a, inset)^{10,23}. At the same time, $\langle R_t \rangle$ exhibited monotonic increase by about 1 Ω with $|V_{Au}|$ corresponding to the temperature rise of up to about 0.3 K

above T_0 (Fig. 4 c). The $\langle R_t \rangle - V_{Au}$ was reproduced in the consecutive sweeps in positive and negative directions indicating stable heat dissipation and diffusion under the relatively slow voltage sweep rate.

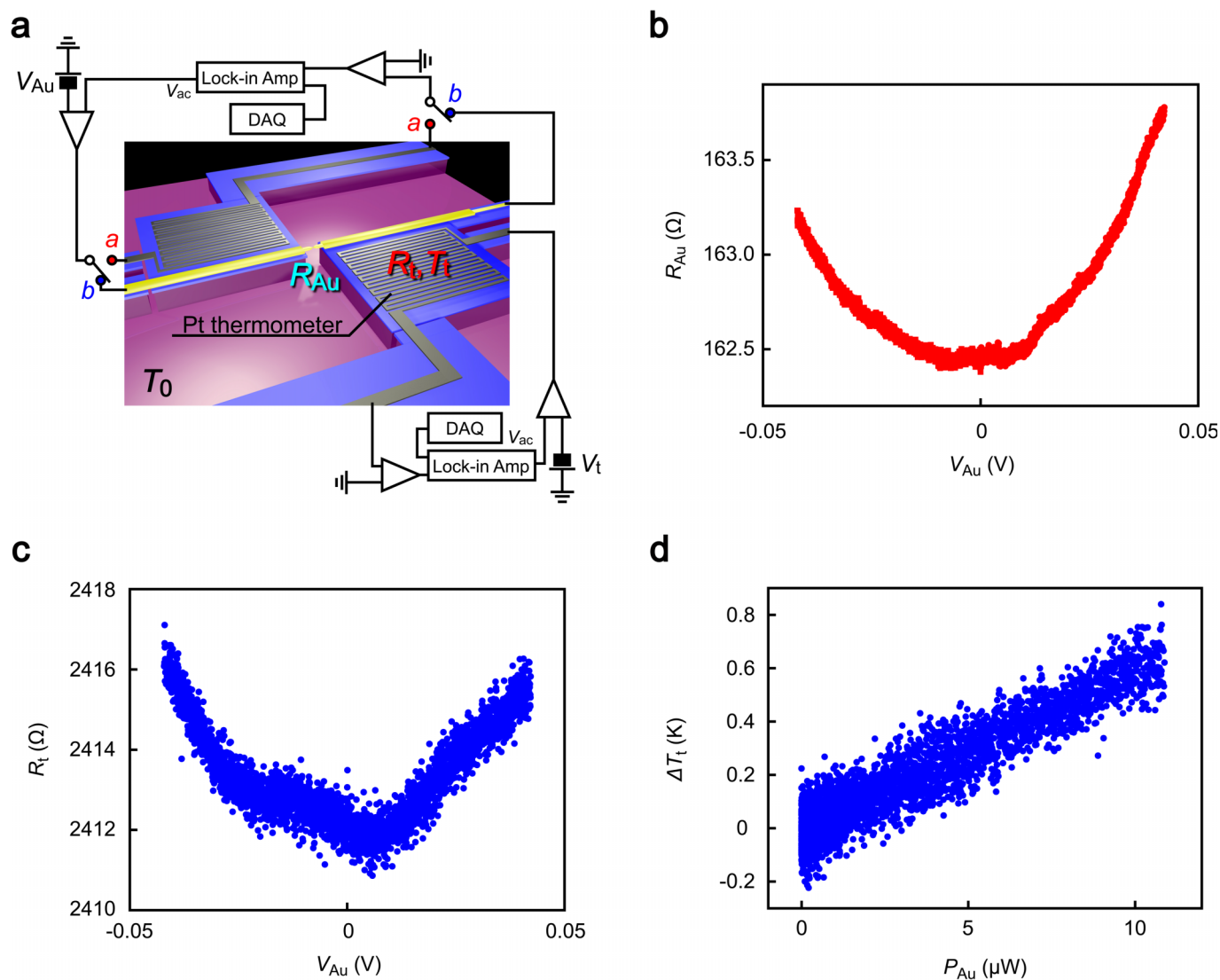


Figure 3 | Electrical heating of a Au nano-junction at $T_0 = 150$ K. (a) A measurement circuit utilized for characterization of Joule heat generated in a Au nano-junction. Bias voltage V_{Au} was applied to the Au nano-constriction and the resistance of the junction R_{Au} as well as that of the thermometer R_t was measured simultaneously. (b) The junction resistance R_{Au} increases with V_{Au} by Joule heating. (c) At the same time, the thermometer resistance R_t also increases. The irregular behaviour of R_t is presumably due to annealing effects on the Au contact microstructure. (d) The local temperature change at the thermometer ΔT_t scales linearly with the power P_{Au} consumed by the junction.

Discussion

It is of interest to explore the underlying physics of the temperature rise at the Pt coil thermometer detected in response to a current flow through a single-atom junction. The positive response of ΔT_t to V_{Au} implies non-negligible heat dissipation in the Au junction. However, unlike the typical Joule heating characteristics observed for the nano-contact shown in Fig. 3 d, $\Delta T_t - P_{Au}$ plots for the single-atom chain reveal nonlinear temperature increase against the input power and an asymmetry with respect to the bias polarity (Fig. 4 c,d). In order to shed light on this peculiar feature, we investigated the onset of the electron-phonon-interaction-derived local heating in the single-atom contact by conducting an inelastic noise spectroscopy^{23–25}. Current noise is characterized here by the standard deviation $\sigma = [\sum_{i=0}^n (I_i - \langle I \rangle)^2 / n]^{1/2}$ calculated from the set of n -point I data acquired at each V_{Au} step during a voltage sweep. Although the feature as a whole is broadened by thermal smearing, we can find stepwise increase of σ with V_{Au} as shown in Fig. S3. The corresponding $d\sigma/dV_{Au} - V_{Au}$ curve shows peaks at around $|V_{Au}| = 0.01$ V (Fig. 4 e). This inelastic spectrum thus suggests an onset of

electron-phonon interactions at $|V_{Au}| \sim 0.01$ V, the corresponding excitation energy of which corresponds to the acoustic phonon modes of Au single-atom chains^{10,26}.

The above results manifest non-negligible local heating in the current-carrying quasi-ballistic single-atom contact that can be a possible cause of the local temperature increase detected by the thermometer. There are two distinct mechanisms responsible for the local heating in atom-sized junctions: electron-phonon and electron-electron scattering. Among these, local ionic heating via electron-phonon scattering fails to explain the bias polarity asymmetry of the $\Delta T_t - V_{Au}$ dependence: T_t starts to increase from 0 V in positive V_{Au} region whereas the temperature rise is suppressed in the low voltage range of -0.04 V $\leq V_{Au} \leq 0$ V at negative bias side, while on the other hand, there is no conspicuous bias polarity dependence of electron-phonon interactions confirmed in the noise spectrum (Fig. 4 e). For electron-electron scattering, it serves to heat up electrons appreciably in a quasi-ballistic nanoscale conductor by the huge current density and affect the bias dependence of the local junction temperature^{4,8,27}. This local electron heating has been

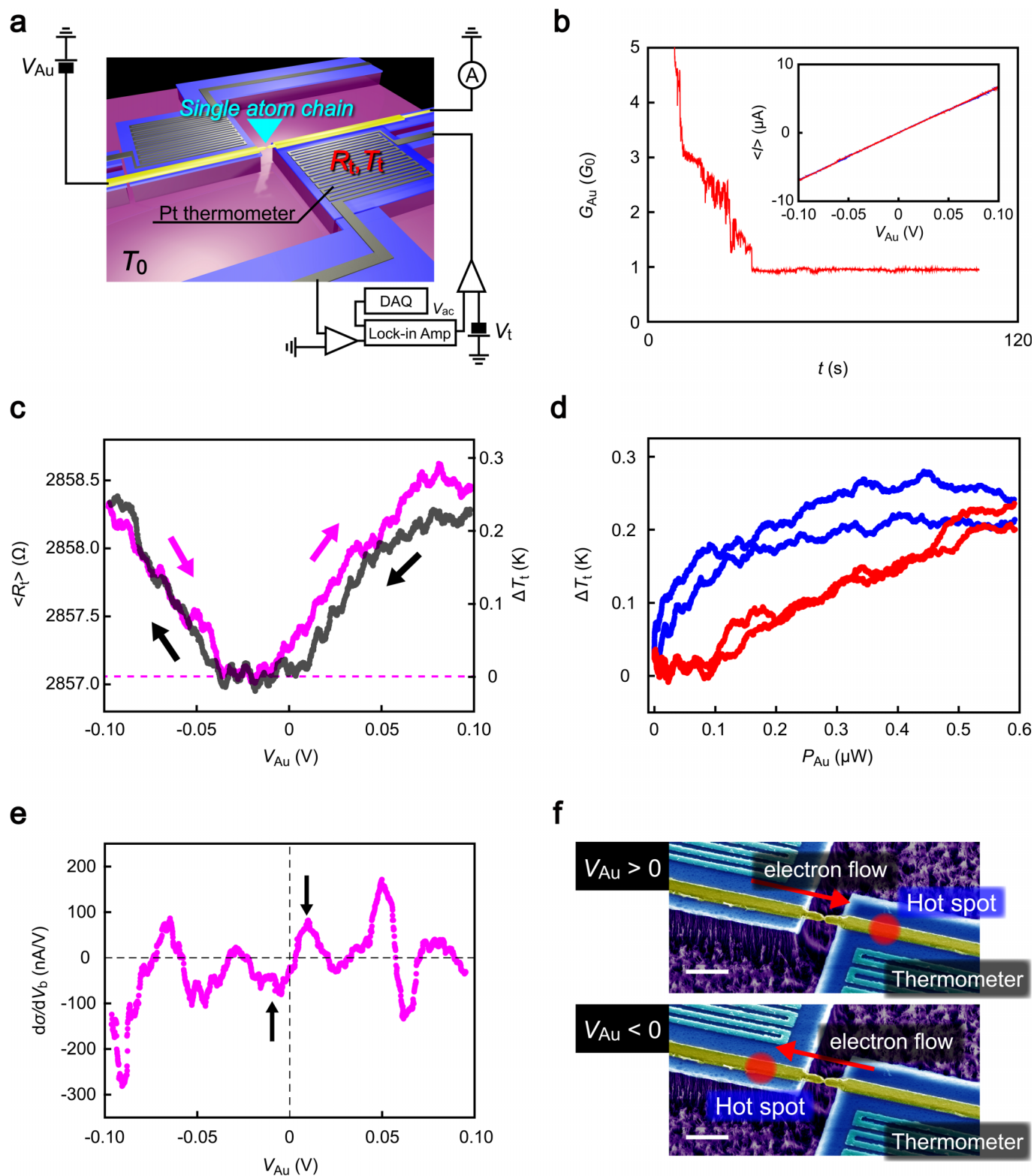


Figure 4 | Characterization of power dissipation in a quasi-ballistic single-atom contact. (a) The measurement set up used for detection of local electrical heating in a Au single atom contact. Bias voltage V_{Au} was swept in a range from -0.1 V to 0.1 V and the resistance R_t of the thermometer was simultaneously recorded. (b) Formation of a Au single-atom wire using the self-breaking technique at $T_0 = 80$ K under $V_{Au} = 0.05$ V. The contact conductance $G_{Au} (= 1/R_{Au})$ exhibits a flat plateau at about $1 G_0$ during mechanical stretching signifying junction thinning to a single-atom size. Inset is the average current-voltage ($\langle I \rangle - V_{Au}$) characteristics measured for a Au single-atom contact. (c) The local temperature change ΔT_t at the thermometer during the voltage sweep on the single-atom junction estimated from the average Pt coil resistance $\langle R_t \rangle$. (d) Plots of ΔT_t with respect to $P_{Au} = V_{Au}^2 / R_{Au}$. Red (blue) dots correspond to ΔT_t at $V_{Au} < 0$ V ($V_{Au} > 0$ V) in (b). (e) The noise spectrum of Au single atom wire. Dashed lines are a guide to the eyes. Arrows point to the lowest peak that represents an onset of local ionic heating in the atomic bridge. (f) Hot electron heating mechanism. A hot spot is generated at the different side of the junction depending on the bias polarity. Scale bars denote $1 \mu\text{m}$.



predicted theoretically to originate a larger current density at the electron flow downstream and accompanied significant electron-phonon scattering there that causes a hot spot at one side of the junction. The asymmetric $\Delta T_t - V_{Au}$ dependence can thus be explained qualitatively by the contribution of this electron heating. However, it is also anticipated that the electron heating effect is less significant compared to the local ionic heating and not detectable in metallic nanocontacts^{4,8,27}. Therefore, although we cannot rule out the possibility, the asymmetric heating in the Au single-atom chain found in the present study may not be attributed to the local electron heating mechanism.

On the other hand, it is more likely that power dissipation by hot electrons is responsible for the electrical heating phenomenon identified through the local temperature measurements here. The accelerated electrons transmit ballistically through Au single-atom junctions and become scattered by phonons at a distance defined by the inelastic mean free path (typically several hundreds of nanometer under low field) and release the kinetic energy there¹⁷. This hot electron heating is thus directional along the electric field; a hot spot is created close to (away from) the thermometer at the electron flow downstream under positive (negative) V_{Au} (Fig. 4 f). As a consequence, the heating effects became too weak to cause a detectable change in T_t at small negative V_{Au} where power dissipation of hot electrons took place at the opposite side of the single-atom contact, since heat transfer to the thermometer becomes less efficient due to the relatively large thermal resistance at the atomic-scale constriction. Meanwhile, the asymmetry of $\Delta T_t - V_{Au}$ curve is becoming less obvious at the high voltage regions (Fig. 4 c). It is anticipated that inelastic scattering length of hot electrons diminishes with V_{Au} because of enhanced probability of multiphonon scattering^{28,29}, thereby shifting the hot spot closer to the junction. As a result, a hot spot generated near the thermometer under positive V_{Au} tends to move away from the thermometer as V_{Au} increases and gives rise to the saturation-like local heating effects at the high biases. In contrast, the hot spot moves closer to the thermometer when sweeping V_{Au} from 0 to -0.1 V, which leads to more pronounced heating effects at high $|V_{Au}|$ in the negative bias regime. Eventually, asymmetry of the hot electron heating effects disappears under high field as hot spot emerges at the vicinity of the Au single atom contact under high field irrespective of the bias polarity, which explains the high-bias ΔT_t behavior in Fig. 4 c. In fact, quantitatively, fraction of the power dissipated in the single-atom chain should be marginal considering the ballistic nature of electron transport³. Therefore, predominant portion of the power is dissipated via inelastic scattering of hot electrons at the current downstream side of the contact bank.

Methods

Fabrication of micro-thermometer-embedded mechanically-controllable break junctions. Micro-thermometer-embedded MCBJs were fabricated as follows (see also Fig. S1). First, a polyimide layer (Pyre-MI, Industrial Summit Technology Co.) of 4 μm thick was spin coated on one side of a phosphorous bronze substrate. Micro-electrodes were fabricated on the polyimide surface using a photo-lithography technique followed by metal deposition (Cr/Au = 2 nm/20 nm) with a radio-frequency magnetron sputtering method and subsequent lift-off (Fig. S1 (a)). Al_2O_3 films of 20 nm thick were then rendered using an electron-beam lithography, radio-frequency magnetron sputtering, and lift-off processes. Subsequently, Au junctions having a narrow constriction with a cross-section of about 100 nm \times 100 nm was formed (a thin Cr layer of 1 nm thick was used for adhesion). After that, Pt coils were prepared, whose thickness and width were 30 nm and 300 nm, respectively. Finally, the sample was exposed to isotropic reactive ion etching with a mixture gas of CF_4/O_2 . As a result, polyimide underneath was removed making the Au and Pt electrodes partially free-standing (Fig. S1 b).

Mechanical break junction system configuration. The micro-thermometer-embedded MCBJ was mounted on the stage of a cryostat in a three-point bending configuration. A piezo-actuator-driven pushing rod was placed at the back of the sample to mechanically bend the phosphorous bronze beam (Fig. 1 c). By doing so, we could narrow the constriction of the Au nanobridge by the necking and form a stable

atom-sized contact (Fig. 1 d)³⁰. After evacuating the chamber to below 10^{-5} Torr, we introduced liquid coolant and cooled the junction.

Pt heater and thermometer calibrations. The platinum thermometers were calibrated by checking the resistance change R_h and R_t of the Pt heater and the Pt resistance thermometer during the cooling process^{21,31}. For this, ac voltage of $V_{ac} = 2$ mV at 1 kHz was applied to the Pt coils and the differential resistance R_{ht} was acquired using two lock-in amplifiers (SR830, Stanford Research Systems Co.) while monitoring the substrate temperature T_0 with a temperature sensor/controller (Scientific Instruments Model 9700) as schematically depicted in Fig. 2 a. We observed linear decrease of R_h with decreasing T_0 from 300 K to 60 K at a rate of $r = 5.8 \Omega/\text{K}$ (Fig. 2 b), which is attributed to mitigated electron-phonon scattering at the low temperatures. Among the samples we fabricated, r as well as the room temperature resistance varied in a range of 4 to 7 Ω/K and 2500 to 3500 Ω , respectively. The scattering of these sensor parameters stem most likely from a difference in the coil geometries and microstructures. We note that this temperature coefficient agrees with the previous experimental reports²¹.

Single-atom contact formation. We imposed a tensile stress on the Au nano-bridge by mechanically bending the MCBJ substrate. By doing so, the junction was elongated by $d = r_{\text{MCBJ}} L$, where d and L are the displacements of the contact and the piezo-element that bends the phosphor bronze beam, respectively. The attenuation factor r_{MCBJ} was $\sim 3 \times 10^{-4}$ estimated by examining an exponential decay of tunnelling current flowing through the vacuum gap between the two MCBJ electrodes¹⁸. As a result, we could break and form a Au junction repeatedly by controlling the substrate bending through manipulation of the piezo-actuator driving voltage. Formation of a single-atom contact was implemented via a resistance-feed-back control of the junction thinning processes³⁰. In this procedure, a fused contact was elongated under a constant voltage of $V_{Au} = 0.05$ V at a predefined stretching rates ranging from 6 nm/s to 6 pm/s while monitoring the conductance $G = 1/R_{Au}$ ¹¹. We observed a gradual decrease of G indicating narrowing of the junction by stress concentration at the constriction and concomitant necking deformation. The conductance trace revealed a staircase-like feature when G is further lowered to below $10 G_0$, and finally demonstrated a flat plateau at around $1 G_0$ right before dropping to zero, where $G_0 = 2e^2/h \sim 77.5 \mu\text{S}$ is the conductance quantum (Fig. 3 a). At this stage, the atom-sized junction undergoes mechanical thinning via atom rearrangements and eventually evolved into a single-atom chain that possesses one fully opened channel for electron transmission¹⁹.

- Cahill, D. G. *et al.* Nanoscale thermal transport. *J. Appl. Phys.* **93**, 793 (2003).
- Pop, E., Sinha, S. & Goodson, K. E. Heat generation and transport in nanometer-scale transistors. *Proc. IEEE* **94**, 1587 (2006).
- Pop, E. Energy dissipation and transport in nanoscale devices. *Nano Research* **3**, 147 (2010).
- Dubi, Y. & Di Ventra, M. Heat flow and thermoelectricity in atomic and molecular junctions. *Rev. Mod. Phys.* **83**, 131 (2011).
- Todorov, T. N. Local heating in ballistic atomic-scale contacts. *Philos. Mag.* **B 77**, 965 (1997).
- Todorov, T. N., Hoekstra, J. & Sutton, A. P. Current-induced embrittlement of atomic wires. *Phys. Rev. Lett.* **86**, 3606–3609 (2001).
- Chen, Y., -C., Zwolak, M. & Di Ventra, M. Local heating in nanoscale conductors. *Nano Lett.* **3**, 1691–1694 (2003).
- D'Agosta, R., Sai, N. & Di Ventra, M. Local electron heating in nanoscale conductors. *Nano Lett.* **6**, 2935–2938 (2006).
- Galperin, M., Nitzan, A. & Ratner, M. A. Heat conduction in molecular transport junctions. *Phys. Rev. B* **75**, 155312 (2007).
- Agrait, N., Untiedt, C., Rubio-Bollinger, G. & Vieira, S. Onset of energy dissipation in ballistic atomic wires. *Phys. Rev. Lett.* **88**, 216803 (2002).
- Tsutsui, M., Kurokawa, S. & Sakai, A. Bias-induced local heating in Au atom-sized contacts. *Nanotechnology* **17**, 5334–5338 (2006).
- Huang, Z. *et al.* Local ionic and electron heating in single-molecule junctions. *Nat. Nanotechnol.* **2**, 698–703 (2007).
- Tsutsui, M., Taniguchi, M. & Kawai, T. Local heating in metal-molecule-metal junctions. *Nano Lett.* **8**, 3293 (2008).
- Ioffe, Z. *et al.* Detection of heating in current-carrying molecular junctions by Raman scattering. *Nat. Nanotechnol.* **3**, 727–732 (2008).
- Schulze, G. *et al.* Resonant electron heating and molecular phonon cooling in single C_{60} junctions. *Phys. Rev. Lett.* **100**, 136801 (2008).
- Ward, D. R., Corley, D. A., Tour, J. M. & Natelson, D. Vibrational and electronic heating in nanoscale junctions. *Nat. Nanotechnol.* **6**, 33–38 (2011).
- Halbritter, A. *et al.* Connective neck evolution and conductance steps in hot point contacts. *Phys. Rev. B* **65**, 045413 (2002).
- van Ruitenbeek, J. M. *et al.* Adjustable nanofabricated atomic size contacts. *Rev. Sci. Instrum.* **67**, 108 (1996).
- Agrait, N., Yeyati, A. L. & van Ruitenbeek, J. M. Quantum properties of atom-sized conductors. *Phys. Rep.* **377**, 81 (2003).
- Schwab, K., Henriksen, E. A., Worlock, J. M. & Roukes, M. L. Measurement of the quantum of thermal conductance. *Nature* **404**, 974–977 (2000).
- Kim, P., Shi, L., Majumdar, A. & McEuen, P. L. Thermal transport measurements of individual multiwalled nanotubes. *Phys. Rev. Lett.* **87**, 215502 (2001).



22. Gao, B. *et al.* In situ transmission electron microscopy imaging of grain growth in a platinum nanobridge induced by electric current annealing. *Nanotechnol.* **22**, 205705 (2011).
23. Tsutsui, M., Taniguchi, M. & Kawai, T. Single-molecule identification via electric current noise. *Nat. Commun.* **1**, 138 (2010).
24. Chen, Y. C. & Di Ventra, M. Effect of electron phonon scattering on shot noise in nanoscale junctions. *Phys. Rev. Lett.* **95**, 166802 (2005).
25. Haupt, F., Novotny, T. & Belzig, W. Phonon-assisted noise in molecular junctions. *Phys. Rev. Lett.* **103**, 136601 (2009).
26. Gawronski, H., Mehlhorn, M. & Margenstern, K. Imaging phonon excitation with atomic resolution. *Science* **319**, 930–933 (2008).
27. D'Agosta, R. & Di Ventra, M. Local electron and ionic heating effects on the conductance of nanostructures. *J. Phys.: Condens. Matter* **20**, 374102 (2008).
28. Yanson, I. K. & Shklyarevskii, O. I. Point-contact spectroscopy of metallic alloys and compounds. *Sov. J. Low Temp. Phys.* **12**, 509 (1986).
29. Persson, B. N. J. & Demuth, J. E. Inelastic electron tunneling from a metal tip. *Solid State Commun.* **57**, 769–772 (1986).
30. Tsutsui, M., Taniguchi, M. & Kawai, T. Atomistic mechanics and formation mechanism of metal-molecule-metal junctions. *Nano Lett.* **9**, 2433–2439 (2009).
31. Shi, L. *et al.* Measuring thermal and thermoelectric properties of one-dimensional nanostructures using a microfabricated device. *J. Heat Trans.* **125**, 881 (2003).

Acknowledgements

T. K. Acknowledges financial support from the Japan Society for the Promotion of Science (JSPS) through its “Funding Program for World-Leading Innovative R&D on Science and Technology”.

Author contributions

M. Tsutsui, T. K., and M. Taniguchi planned and designed experiments. M. Tsutsui and M. Taniguchi fabricated MCBJ devices, exhibited single-molecule conductance measurements, and performed data analyses. M. Tsutsui, T. K., and M. Taniguchi co-wrote paper.

Additional information

Supplementary information accompanies this paper at <http://www.nature.com/scientificreports>

Competing financial interests: The authors declare no competing financial interests.

License: This work is licensed under a Creative Commons Attribution-NonCommercial-ShareAlike 3.0 Unported License. To view a copy of this license, visit <http://creativecommons.org/licenses/by-nc-sa/3.0/>

How to cite this article: Tsutsui, M., Kawai, T. & Taniguchi, M. Unsymmetrical hot electron heating in quasi-ballistic nanocontacts. *Sci. Rep.* **2**, 217; DOI:10.1038/srep00217 (2012).